Hybrid Heterogeneous Integrated Wireless Sensor Devices with Multilayer Composite Films

Xiaorui Liang *, Lei Zhang , Qiulin Tan

Posted Date: 12 May 2025

doi: 10.20944/preprints202505.0882.v1

Keywords: high temperature; wireless; hybrid heterogeneous integrated; multilayer composite films; HTCC

 doi:10.20944/preprints202505.0882.v1

Article

Hybrid Heterogeneous Integrated Wireless Sensor Devices with Multilayer Composite Films

Xiaorui Liang [1,2], Lei Zhang [2] and Qiulin Tan [2,*]

[1] School of Electronic and Information Engineering, Taiyuan University of Science and Technology, Taiyuan 030024, China
[2] Key Laboratory of Micro/nano Devices and Systems, Ministry of Education, North University of China, Taiyuan 030051, China
* Correspondence: tanqiulin@nuc.edu.cn

Abstract: To realise the real-time monitoring of safety and health of military and industrial devices, such as aerospace vehicles, aero-engine blades, and boilers in thermal power plants, within the operating temperature range of ≥1400°C, this study proposed a miniaturised, integrated, high-thermal-stability wireless sensor device. This study analysed the influence of temperature on the interdigital electrode of surface-acoustic-wave temperature sensors with different structures of a bare electrode, single-layer protective film, and multilayer composite film. The exposed electrode exhibited high thermal stability at a high temperature of 1000°C, but the sensor failed at 1250℃. To achieve health monitoring of military and industrial devices in a high-temperature environment of >1400℃, a multilayer protective film structure of aluminium oxide/aluminium nitride/alumina was proposed. The device can operate at up to 1400℃ with a sensitivity of 7.41 KHz/℃. The electrode protection function improved working temperature. To realize real-time monitoring, a wireless sensor device, that is, a hybrid heterogeneous integration of high-temperature co-fired ceramic (HTCC) antenna and lanthanum silicate-based surface acoustic wave with a multilayer composite film, was proposed. The wireless device could operate in from room temperature to 1400°C and could be maintained at a constant temperature of 1400°C for 2 h with a repeatability error of 12.67%. The integrated structural design of the device and antenna was realized, and the miniaturisation of high-temperature wireless devices was achieved through. This study provides important guidance for the real-time monitoring of military and industrial device safety in high-temperature and other harsh environments.

Keywords: high temperature; wireless; hybrid heterogeneous integrated; multilayer composite films; HTCC

1. Introduction

The speed of hypersonic-designed aircraft is rapidly increasing. When the aircraft is flying at a high speed, aerodynamic heat is generated because of the fluid flowing through the fuselage. This aerodynamic heat can cause irreversible damage to the aircraft, reducing its structural strength and rigidity and resulting in ablation of its structural shape and elastic deformation of the fuselage to a certain extent, which can severely affect the normal flight and safety of the aircraft[1,2]. Aerospace engine turbine blades operate in harsh environments with ultra-high temperatures, strong airflow, and severe vibrations. The surface temperature of the turbine blades reaches 1400°C, which makes the aircraft extremely vulnerable to damage or even cracks. The quality of the turbine blades directly determines the performance of the aerospace engine[3,4]. To prevent the thermal damage of the blades, real-time temperature monitoring must be realised during their rotation[5–7]. The flame temperature of the boilers used in thermal power plants can exceed 1600°C, which can damage components, considerably reducing their service life and safety[8]. It is impossible to determine the operating status of the boilers in real time, and there is a lack of high-temperature real-time

 doi:10.20944/preprints202505.0882.v1

monitoring mechanisms and equipment for them. Therefore, for the real-time monitoring of the safety of aircraft, turbine blades, and boilers used in thermal power plants in harsh environments, high-temperature wireless sensors with miniaturisation, integration, and high reliability must be urgently developed. Recently, surface acoustic wave (SAW) devices have been applied to the research of high-temperature sensors due to their small size, high precision, good stability in an ultra-high-temperature environment, and wireless passive remote sensing[9–12]. SAW devices use the characteristics of acoustic-electric transducers for various processes on the acoustic signals propagating on the surface of piezoelectric material substrates to perform different applications. Common piezoelectric materials include quartz[13,14], $LiNbO_3$[15,16], and $LiTaO_3$[17,18], however, they are difficult to be operated at >1000°C[19]. A langasite (LGS) crystal has a high melting point (1470°C); high electromechanical coupling coefficient (32%), which is approximately two to three times that of quartz (0.14%); low sound scattering; small body-wave interference; and no phase transition before the melting point. However, it still exhibits the piezoelectric effect and acts as an oxide. In a vacuum environment, LGS crystals can undergo loss of oxygen and gallium[20,21], which leads to their decomposition[22]. However, the colour of an LGS crystal does not change in air. Therefore, LGS is a promising high-temperature-resistant piezoelectric material[23,24] and especially suitable for the application of high-temperature SAW sensors in the air atmosphere.

Considerable research has been conducted for high-temperature devices based on LGS substrates for sound surface waves, and because Pt has a high melting point (1772°C), is chemically stable, is insoluble in strong acid and alkali solutions, and does not oxidise with stability before the melting point, it has been extensively used as an electrode to prepare high-temperature devices. For example, Li et al. studied the application of the Pt/Ti/LGS structure in high-temperature sensors at an operating temperature of 50°C–650°C[25]. Peng et al., prepared an SAW sensor using Pt as the electrode, where two stainless-steel tubes bonded to a ceramic substrate with high-temperature cement as a $\lambda/2$ dipole antenna. Then, the dipole antenna was connected to the interdigital transducer IDT transmitter terminal of an LGS-based SAW device by using a painted Pt/silver conductor paste for a high-temperature wireless test. The working temperature in the experiment reached 700°C[26]. Bulk diffusion occurs in metallic materials near the Taman temperature[27], which is the temperature at which reactants begin to exhibit considerable diffusion. For different substances, the Taman temperature and melting point are related. The Taman temperature of metals is 0.3–0.4 Tm. This indicates that the Taman temperature of Pt is approximately 750°C[28,29]. In addition, the metal Pt electrode agglomerates near the Taman temperature, but there are no isolated Pt particles. After maintaining the temperature at 1000°C for 1 h, the isolated Pt particles can be formed, resulting in the destruction of the electrode structure and loss of conductivity[30]. To improve the high-temperature resistance of the device in harsh environments, such as high temperature, the agglomeration of the Pt electrode at high temperatures must be inhibited. To address the aforementioned problems, a SAW resonator, which used the PT-RH/HfO_2 IDT electrode and Al_2O_3protective coating and worked for more than 2 h at 1100°C, was developed by the University of Maine [31]. The University of Electronic Science and Technology of China adopted an Al_2O_3/Pt/ZnO/Al_2O_3 composite film as the electrode, which maintained stable resonance even after 12 iterations of 1100°C annealing. A SAW resonator exhibits the strongest high-temperature resistance[32]. In the early stage, the research group used an Al_2O_3 thin film as the Pt electrode protection layer, and an LGS-based SAW temperature sensor was realised at 1300°C[33]. Although the aforementioned studies could provide the high-temperature-resistance performance of the device, health monitoring of space vehicles, aero-engine blades, thermal power plant boilers, and other wireless sensor parts could not be achieved. In addition, current research could not achieve miniaturisation and an integrated design in a narrow space.

In this study, a bare electrode maintained good performance at 1000°C, but at 1250°C, the surface of the Pt electrode exhibited agglomeration, and the structure of the forked finger broke, which caused sensor failure. To improve the device's operating temperature range, the monolayer, protective AlN film, which effectively suppressed the diffusion of Pt atoms caused by a high-temperature environment, was analysed. However, the sensor failed after being maintained 1300°C

 doi:10.20944/preprints202505.0882.v1

for 2 h. Thus, an Al_2O_3/AlN/Al_2O_3 multilayer composite film structure was proposed to further improve the high-temperature resistance.

In addition, a dipole antenna is currently used for wireless testing of most high-temperature devices, and a small integrated design of antenna and device has not yet been realised. Therefore, based on the Al_2O_3/AlN/Al_2O_3 multilayer composite film structure, this paper proposes a hybrid heterogeneously integrated wireless sensor with high-temperature co-fired ceramic (HTCC) antenna and an LGS-based SAW device with a multilayer composite film, realising the miniaturisation of wireless integrated devices. The Al_2O_3/AlN/Al_2O_3 multilayer composite film is used as the electrode protection layer, and an HTCC inverted-F antenna is used as the antenna. The SAW sensor and HTCC antenna realise heterogeneous bonding. The wireless sensor can be tested wirelessly at 1400℃ and maintained at this temperature for 2 h, exhibiting a suitable performance. This experiment realises a miniaturised and integrated high-temperature-resistant wireless sensor, which has significant advantages over traditional wired active devices and wireless passive sensor devices based on high-temperature-resistant materials for testing in high-temperature-confined and other harsh environments. In addition, it can address the problems of real-time safety monitoring of aircraft, turbine blades, and thermal power plant boilers under harsh environments, such as high temperatures.

2. Experiment

2.1. Preparation of Multilayer Composite Film Structure

Figure 1(a) shows a schematic diagram of an electrode protection layer–multilayer composite film structure, and Figure 1(b) shows its cross-sectional morphology. The composite structure is realised on the surface of a saw interdigital electrode and a reflective grid prepared on the LGS substrate. First, a 20-nm-thick adhesive Cr layer and a 200-nm-thick Pt metal electrode were deposited on the LGS substrate by magnetron sputtering. Then, a 50-nm-thick Al2O3, 50-nm-thick AlN, and 100-nm-thick Al2O3 films were deposited on the Pt electrode surface by pulsed laser deposition (PLD). The deposition laser intensity was 300 mJ, the laser frequency was 5 Hz, and the deposition temperature was 200℃. The hierarchical structure can be seen in Figure 1(b). The prepared temperature sensor with the multilayer composite film was annealed at a high temperature to eliminate its internal stress and improve the device stability. Figure 1(c) shows the cross-sectional morphology of the structure after sintering. By comparing the morphology of the structure before sintering (Figure 1(b)) with that after sintering (Figure 1(c)), the structure after sintering was found to be significantly thinner.

 doi:10.20944/preprints202505.0882.v1

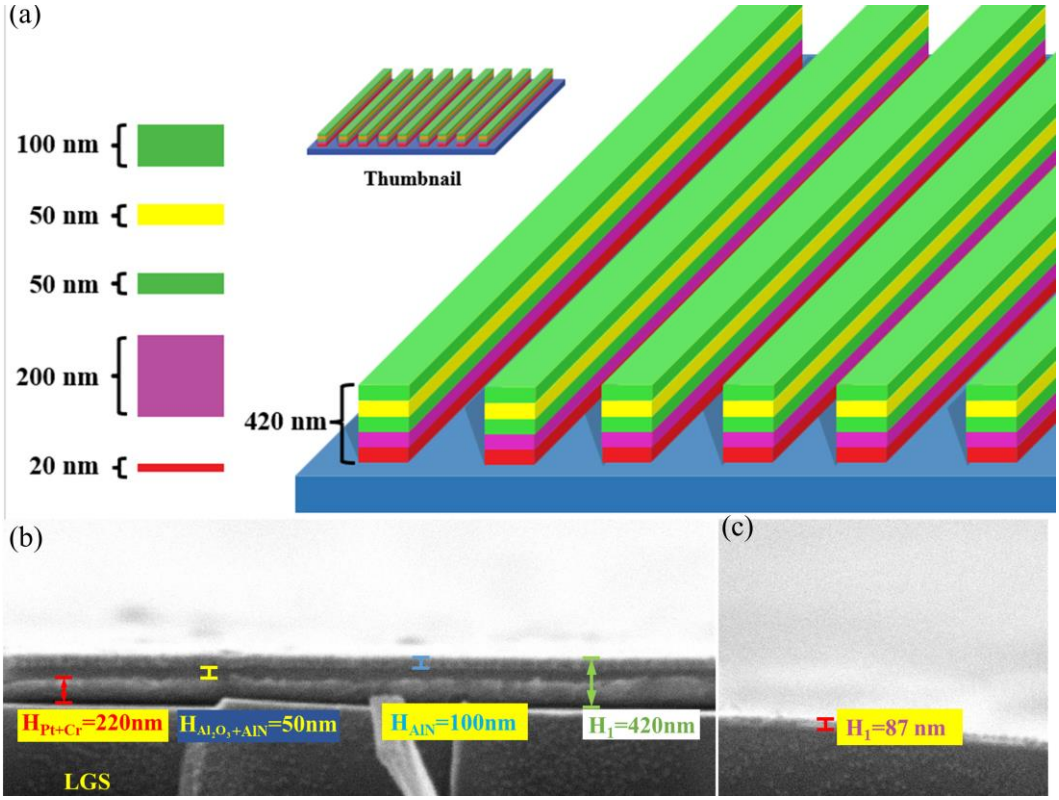

Figure 1. Structure of the multilayer composite film. (a) Schematic of the multilayer composite film. (b) Cross-sectional morphology of the multilayer composite film. (c) Cross-sectional morphology of the multilayer composite film after sintering.

2.2. Manufacturing of HTCC Antenna

The HTCC antenna structure is shown in Figure 2. Figure 2(a) and (b) show the front and reverse views of the antenna structure designed by simulation with HFSS simulation software. Figure 2(a) shows that the front side of the inverted F-type antenna structure presents the graphic antenna structure and ground plate. Figure 2(b) shows that the reverse side of the inverted F-type antenna structure contains the ground plate and notch, which is designed according to the size of the SAW temperature sensor (slightly larger than the sensor size). The dimensions of the antenna are 24 mm×24 mm ×1 mm. Figure 2(c) shows the antenna simulation analysis curve. According to the antenna design document of CYPRESS[34], return loss (RL) refers to the incident power divided by the reflected power (Equation 1), and its value ranges between 0 dB and infinity. The larger the RL, the better is the antenna matches the sensor. When infinity approaches infinity, it indicates a complete match. The closer it is to 0, the more serious and worse is the reflected signal, and the total reflection is 0. That is, the smaller S11, the higher is the transmission efficiency of the antenna. In general, an antenna with RL ≥ 10 dB (equivalent to S11 ≤ -10 dB) exhibits effective transmission. As shown in Figure 2(c), the RL of the experimentally designed antenna (-43.16 dB) is less than or equal to -10 dB, which meets the design requirements of the antenna. The bandwidth of the antenna is approximately 10 MHz, and its frequency is approximately 306 MHz; the voltage standing wave ratio (VSWR) is approximately 1:1; thus, it is close to a travelling wave and exhibits ideal transmission characteristics. Figure 2(d) shows the directional diagram of a 3D antenna, which has a gain of 0.035 dBi.

 doi:10.20944/preprints202505.0882.v1

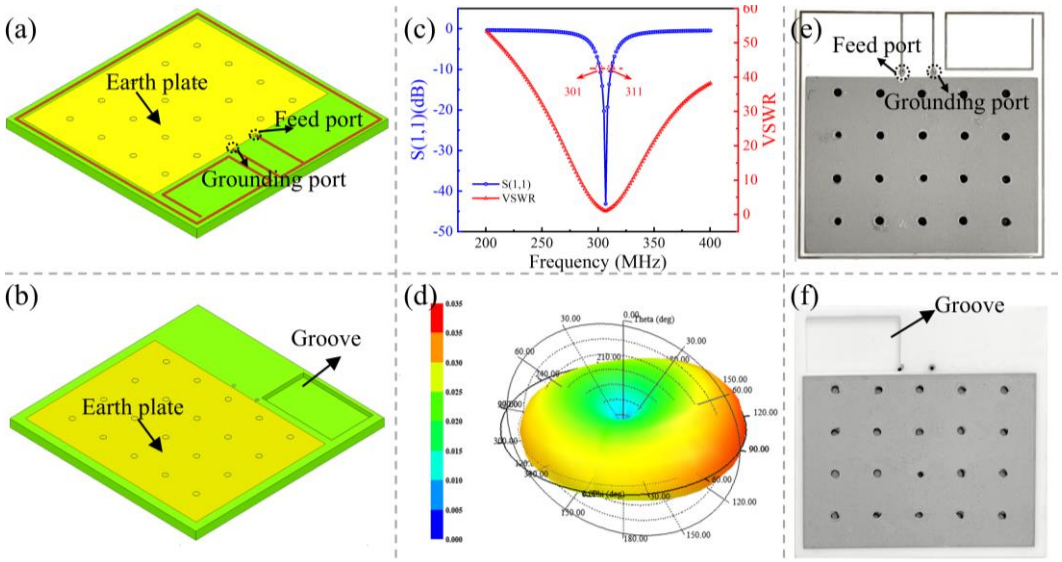

Figure 2. HTCC antenna. (a) The front side of the simulated 3D structure of the antenna. (b) The reverse side of the simulated 3D structure of the antenna. (c) The curve of the antenna simulation analysis. (d) The 3D antenna pattern. (e) The front side of the actual antenna. (f) The reverse side of the actual antenna.

$$\mathrm{R}\,L(dB) = 10\log\left(\frac{P_{incident}}{P_{reflected}}\right) \quad (1)$$

In this study, the HTCC antenna is manufactured according to the simulation design structure. The physical object is shown in Figure 2(e) and (f). The experimental process is as follows. (1) A raw porcelain belt is prepared. (2) A laser drilling machine is used to drill positioning holes and lead connection holes at the four corners of the alumina raw ceramic belt diaphragm, and the raw ceramic belt is accurately placed on the lamination die through the positioning holes, in which the lower four layers of the raw ceramic belt are slotted. (3) In the lamination process, the sacrificial layer is filled into the slot. (4) Lamination is performed. (5) Sintering of the raw porcelain substrate is performed, and (6) screen printing and sintering are performed. The specific production process is shown in Figure 3.

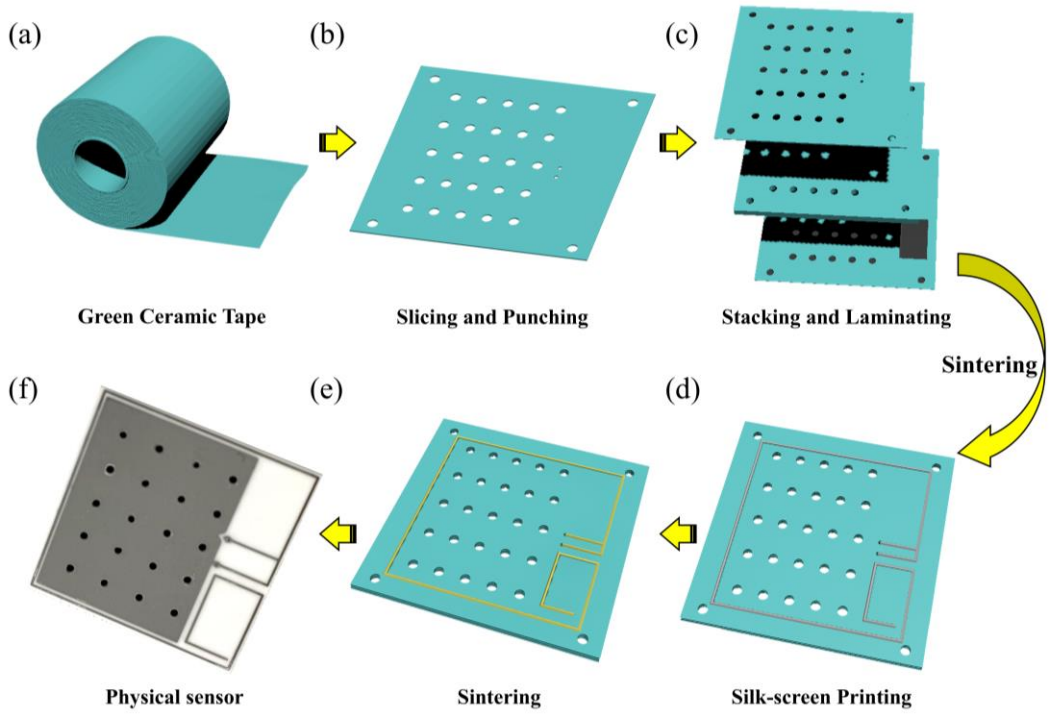

 doi:10.20944/preprints202505.0882.v1

Figure 3. Manufacturing process of HTCC antenna.

2.3. Integrated Manufacturing

Sections 2.1 and 2.2 showed the manufacturing process of the SAW temperature sensor and HTCC, respectively. To realise miniaturisation and integration of high-temperature-resistant wireless sensor parts, the devices manufactured in Sections 2.1 and 2.2 were mixed and heterogeneously integrated in this experiment, as shown in Figure 4. First, the bottom of the recess of the HTCC antenna structure, shown in Figure 2(f), was coated with alumina high-temperature ceramic adhesive. Then, the SAW temperature sensor was embedded in the recess. As a result, the sensor and antenna achieved heterogeneous indirect bonding. Finally, the two electrical extremes of the SAW temperature sensor were connected to the feed port and ground port of the antenna with a Pt wire to achieve heterogeneous integration of the antenna and sensor. Compared to the existing research, the integrated design and manufacturing conducted in the present study considerably reduced the antenna size, which can better realise wireless passive temperature monitoring in a high-temperature and narrow space. In addition, the sensor can be integrated with the antenna structure to facilitate batch processing.

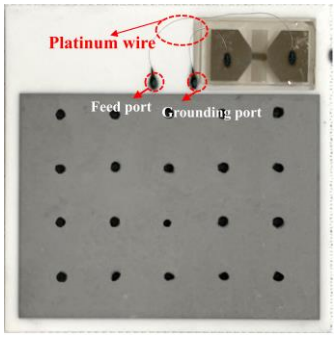

Figure 4. Integrated structure of HTCC base and SAW temperature sensor.

3. Results and Discussion

3.1. High-Temperature Test and Analysis Without Protective Layer

In this study, a SAW sensor was prepared using Cr as the bonding layer. Chromium exhibits a high melting point (1907℃) and slow and stable oxidation under red heat. Figure 5(a) shows the surface morphology of the interdigital electrode of the SAW sensor, with the Pt/Cr/LGS structure prepared with Cr as the bonding layer after high-temperature annealing at 1000℃. The figure shows that the Pt electrode surface is relatively flat with a little bulge, and the interdigital electrode is not broken. Figure 5(b) shows that the sensor with this structure exhibits suitable performance within 1000℃.

 doi:10.20944/preprints202505.0882.v1

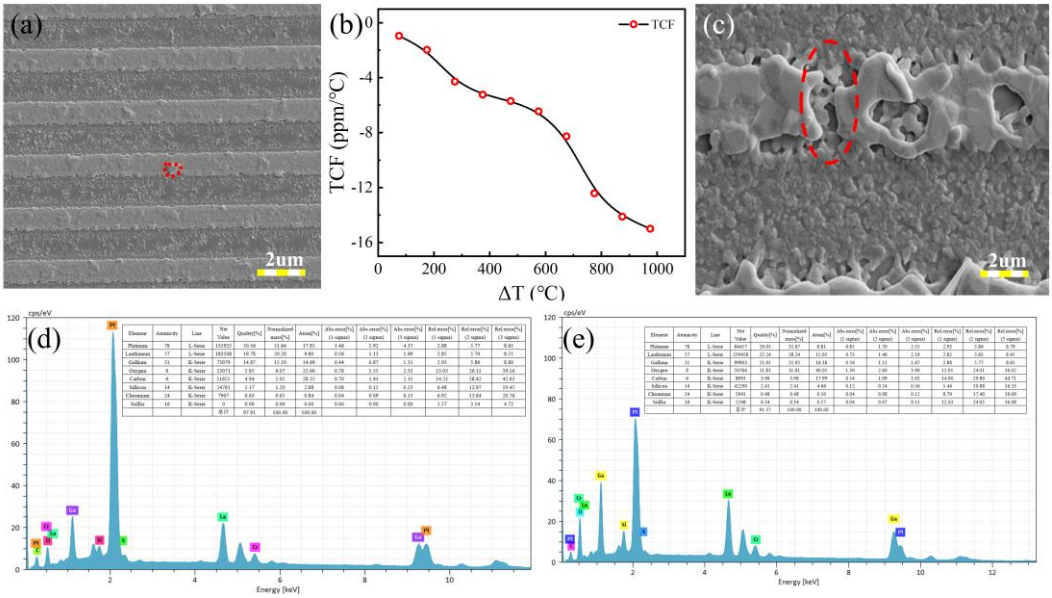

Figure 5. (a) Surface morphology of the forked finger electrode with Pt/Cr/LGS structure. (b) Frequency temperature coefficient. (c) Surface morphology of the forked finger electrode at 1250°C. (d) EDS energy spectrum analysis before high-temperature annealing. (e) EDS energy spectrum analysis after high-temperature annealing at 1250°C.

When the device operates at 1250℃, the Resonance signal increases suddenly. Figure 5(c) shows the surface topography of the device at 1250℃. Here, an evident agglomeration phenomenon occurs on the surface of the Pt electrode, which fractures the cross-finger electrode, and therefore, leads to sensor failure. The energy-dispersive X-ray spectroscopy (EDS) analysis of Pt/Cr/LGS structured SAW devices before and after annealing at 1250℃ is performed, as shown in Figure 5(d) and (e). A comparison of the two figures shows that the element species and atomic number of the device remain constant before and after annealing at high temperature, but the mass ratio of the Pt element changes and the mass decreases by 21.59%. The mass of the Pt element is attenuated under high temperature, which generates the agglomeration phenomenon on the Pt electrode surface (Figure 5(c)).

3.2. High-Temperature Test Analysis of Single-Layer Protective Film

As the sensor with only Pt electrode failed at 1250°C, the device could not operate stably in a high-temperature environment. Therefore, experiments were conducted to deposit an AlN film on the surface of the forked finger electrodes as a protective layer, and 200-nm-thick AlN films were prepared by PLD at a deposition temperature of 200°C. In addition, experiments were conducted to anneal the SAW resonator at 1300°C three times.

Figure 6(a) and (b) show EDS spectrum analysis of high-temperature sensors before annealing and after three times high-temperature annealing at 1300℃. According to the analysis shown in Figure 6(a) and (b), the mass of the Pt element decreases by 10.98% after high-temperature annealing. Compared to the sensor without a protective layer (as shown in Figure 5 (d) and (e)), the Pt element undergoes a slight mass change. The AlN film effectively inhibits the attenuation of the Pt element mass caused by high-temperature annealing.

 doi:10.20944/preprints202505.0882.v1

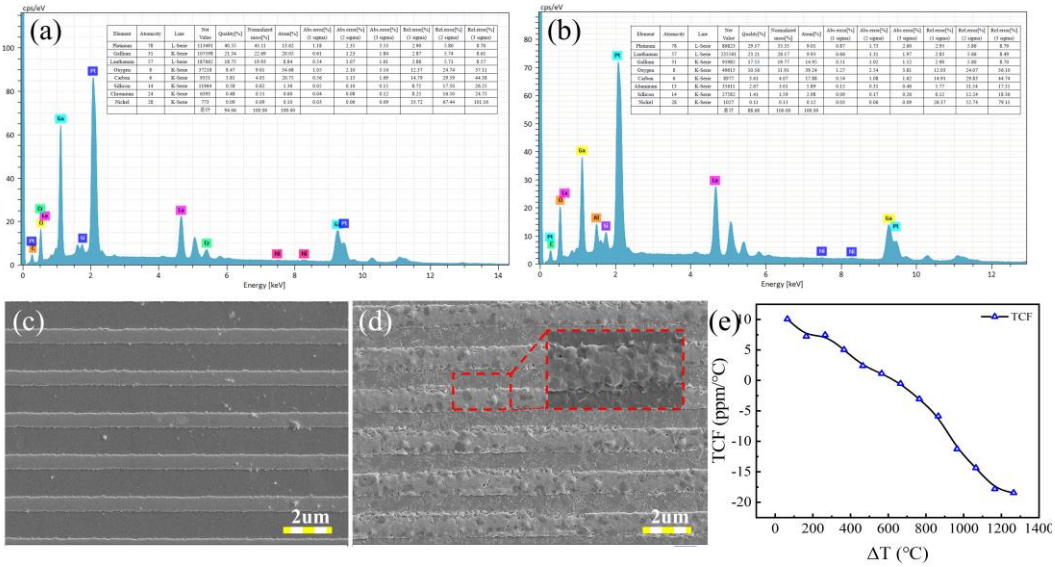

Figure 6. (a) EDS spectra before high-temperature annealing. (b) EDS spectra after high-temperature annealing at 1300℃. (c) Surface topography of 200-nm-thick AlN film on the interdigital electrode before annealing. (d) Surface topography of 200- nm-thick AlN film on the interdigital electrode after three times annealing at 1300℃. (e) Frequency temperature coefficient.

3.3. High-Temperature Test Analysis of Multilayer Protective Film

For the temperature sensor pieces mentioned in sections 3.1 and 3.2, the Pt metal electrodes migrate in the high-temperature environment, forming agglomerates and resulting in reduced sensor conductivity, and thus, sensor failure. Spacecraft, aero-engine blades, and thermal power plant boilers cannot achieve health monitoring within the normal operating range. Therefore, high-temperature-resistant electrodes operating in a high-temperature environment need to be urgently developed. AlN is a suitable thermal shock material with good thermal conductivity and small thermal expansion coefficient; moreover, it has a strong ability to resist molten metal erosion. The α-alumina is the most stable phase of all forms of alumina, with high-temperature-resistant inertia, which is conducive to reducing oxygen atoms' escape. Al_2O_3 and AlN are electrode protection materials with promising application prospects. Therefore, a composite multilayer membrane structure Al_2O_3/AlN/Al_2O_3 is proposed, as shown in Figure 1, with a thickness of 200 nm. The SAW resonator was annealed at 1400℃ for three times. Figure 7(a) shows the thermal expansion coefficient analysis[35]. The point on the dL/L_0 curve represents the ratio (or percentage) of the total length change value of the sample at this temperature to the initial length at room temperature. The critical point at which the slope of the dL/L_0 curve changes from gradually increasing (gradually steeper) to gradually decreasing (gradually flat) is the inflection point, which represents the softening temperature[36]. The samples were analysed with Pt electrodes coated with multilayer composite films (Al_2O_3/ALN/Al_2O_3). Only the inflection point of the LGS wafer was at 1327°C; the inflection point of the LGS wafer with Pt electrodes was at 1317°C. The inflection point of the multilayer composite film (Al_2O_3/ALN/Al_2O_3) was at 1310°C, which shows that the device was highly stable within 1300°C without softening. As shown in Figure 7(a), the curve in the range of 150-1300℃ is nearly linear and exhibits thermal stability. The slope of the curve in this range is the average thermal expansion coefficient. According to the curvature, only the curvature difference between the LGS wafer and Pt electrode coated with multilayer composite film (Al_2O_3/AlN/Al_2O_3) is small. The thermal expansion coefficient of platinum electrode coated with multilayer composite film (Al_2O_3/ALN/Al_2O_3) is closer to that of LGS wafer only, which reduces the error caused by the difference in the thermal expansion coefficient. Figure 7(b) shows that the sensor frequency decreases parabolically with an increase in temperature. The sensitivity is 7.41 KHz/℃. Compared to the single-layer protective film shown in section 3.2, the device's sensitivity is improved.

 doi:10.20944/preprints202505.0882.v1

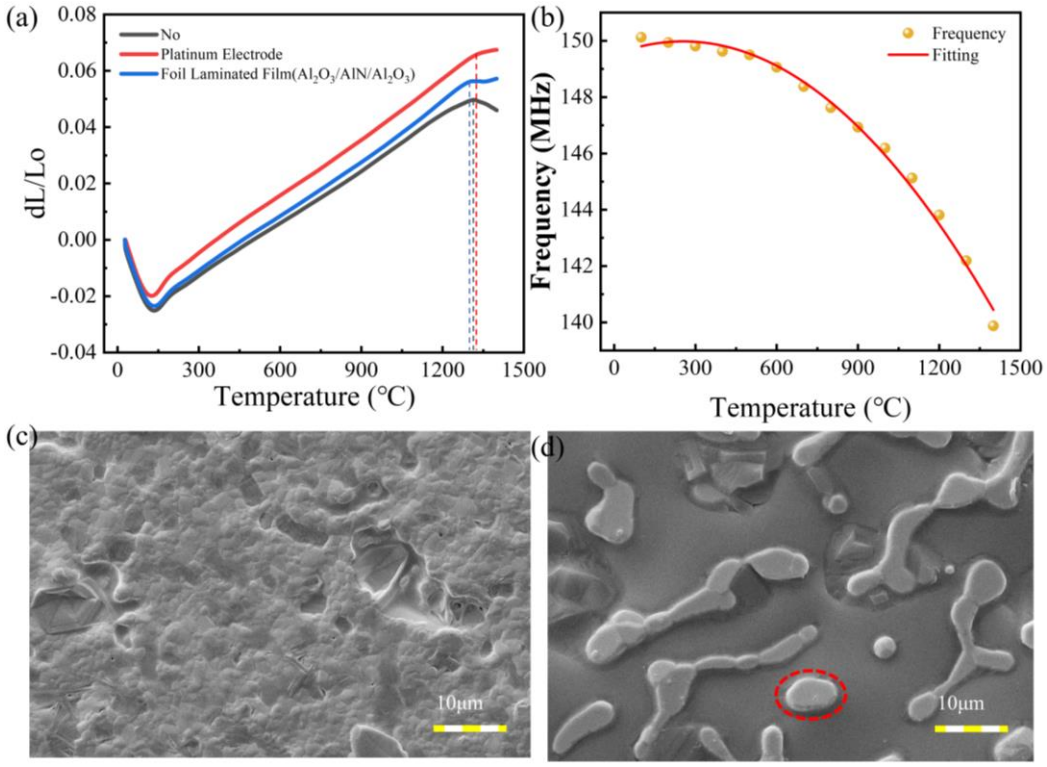

Figure 7. (a) Thermal expansion coefficient analysis. (b) Temperature–frequency curve. (c) Surface topography after first annealing at 1400℃ for 2 h. (d) Surface topography after three times annealing at 1400℃ for 2 h.

Figure 7(c) shows the surface morphology of the sensor after the first annealing at 1400℃ for 2 h. The surface is relatively flat without cracks, lumps, and other phenomena; Figure 7(d) shows the surface morphology after 2 h and three times annealing at 1400℃. Independent agglomerates are formed on the surface, resulting in an incomplete and discontinuous film surface and sensor failure. A protective film of the Al_2O_3/AlN/Al_2O_3 multilayer composite structure is deposited on the surface of the platinum electrode, which can effectively inhibit the agglomeration of platinum atoms, play a protective role, and improve the working temperature.

3.4. Integration Test Analysis

The test environment of the integrated structure of HTCC antenna and SAW temperature sensor is shown in Figure 8. The sensor and transmitter antenna are placed inside the muffle furnace, the receiver antenna is placed outside the furnace, and the distance between the receiver antenna and transmitter antenna is 15 cm. The muffle furnace is set to heat up at a rate of 100°C every 10 min.

 doi:10.20944/preprints202505.0882.v1

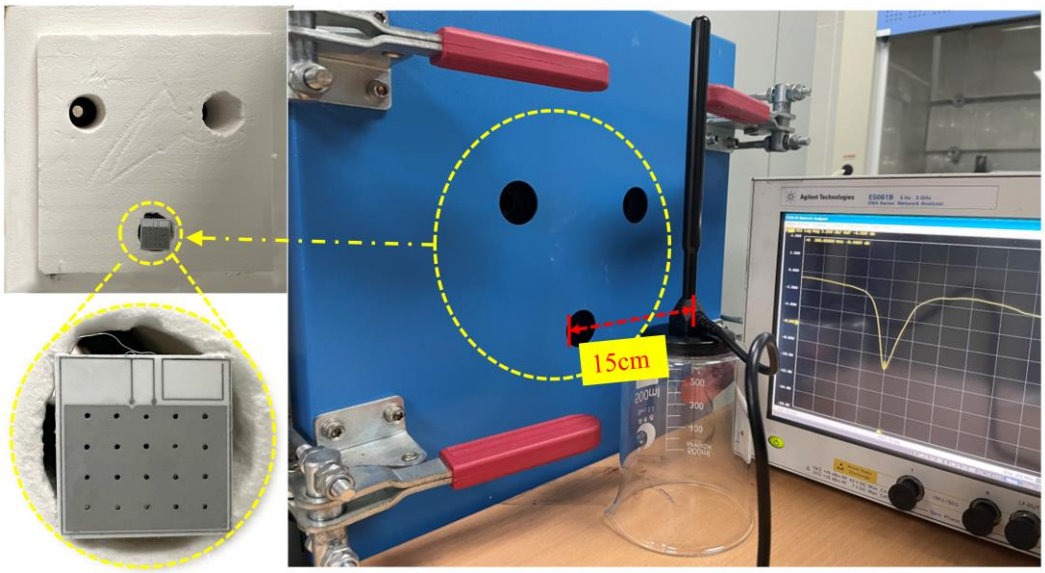

Figure 8. Wireless test environment diagram.

Figure 9(a) shows the temperature coefficient of frequency (TCF) of the HTCC antenna with SAW temperature sensor integrated structure in the within approximately 1400°C. TCF indicates the thermal stability of the resonator; when the temperature changes, TCF is negative, its frequency drifts in the direction of decreasing frequency with increasing temperature, and the amount of change in the resonant frequency is 40.03 ppm/℃ within approximately 1400°C. Figure 9(b) shows the thermal expansion coefficient of the sensor held at 1400℃ for 2 h, and Figure 9(c) shows that of the sensor held at normal temperature to 1400℃ for 2 h. The figure shows that the thermal expansion coefficient remains linear in the heating stage from room temperature to 1400℃, and its inflection point occurs before the insulation stage. However, dL/L0 is linear and exhibits good thermal stability. Figure 9(d) and (e) shows the test results of the antenna without sensor structure in a high-temperature environment. As shown in Figure 9(d), the frequency change of the antenna is 1.0625 MHz, which is relatively small. As shown in Figure 9(e), the TCF changes to 2.43 ppm/℃, close to 0. The resonator has exhibits thermal stability. Therefore, temperature has no influence on the antenna structure. In addition, the effect of temperature on the antenna structure in a high-temperature environment does not significantly impact the resonant frequency drift of the integrated structure. Figure 9(f) analyses the repeatability error of the integrated structure; with an increase in temperature, the repeatability error first decreases and then increases, and the maximum error is 12.67%.

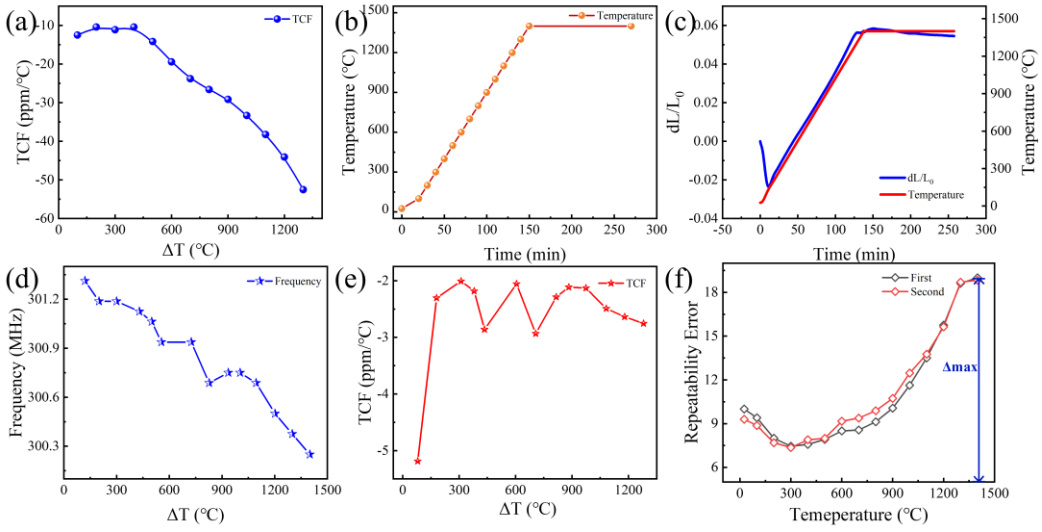

 doi:10.20944/preprints202505.0882.v1

Figure 9. (a) Test results of integrated structure of HTCC antenna and SAW temperature sensor. (b) Test results of HTCC antenna. (c) Analysis of thermal expansion coefficient. (d) error analysis.

4. Conclusions

To achieve real-time monitoring of the safety of aircraft, turbine blades, and thermal power plant boilers in harsh environments, such as high temperatures, this paper proposes a hybrid heterogeneously integrated wireless sensor device with HTCC antenna and LGS-based sound surface wave with a multilayer composite film, which exhibits miniaturisation, integration, and high-temperature stability, realising real-time monitoring of the safety of military and industrial devices in harsh environments. The following conclusions were drawn:

(1)The bare electrode exhibits good thermal stability and high-temperature resistance at 1000°C, but at 1250°C, the mass of the platinum element decreases and clumps form on the surface of the electrode, leading to the fracture of the forked finger electrode and causing the sensor failure.

(2)The single-layer protective AlN film was analysed. Compared to the bare electrode, it not only effectively inhibited the agglomeration of platinum atoms and played a protective role, but the operating temperature also reached 1300°C, which improved the device sensitivity by 2.89 KHz/°C.

(3)Further study of multilayer, protective alumina/aluminium nitride/aluminium oxide film indicated that the device can operate up to 1400°C with a sensitivity of 7.41 KHz/°C. The protective film's multilayer composite structure effectively suppressed the platinum electrode's agglomeration; it plays a protective role and increases the operating temperature.

(4)An HTCC antenna and LGS-based SAW with multilayer composite film heterogeneously integrated wireless sensor device were studied. The wireless device could operate in the temperature range of room temperature to 1400°C and could be maintained at a constant temperature of 1400°C for 2 h for two repeatability tests with a maximum repeatability error of 12.67%. Furthermore, the integrated structural design of the device and antenna was realised, which broke through the miniaturisation of wireless devices and addressed the problem of real-time monitoring of military and industrial device security in high-temperature and other harsh environments.

Author Contributions: Conceptualization, X.L. and L.Z.; methodology, X.L.; software, X.L.; validation, L.Z., Q.T. and Z.Z.; formal analysis, X.L.; investigation, X.L. resources, X.L. and L.Z.; data curation, L.Z., Q.T.; writing—original draft preparation, X.L.; writing—review and editing, X.L., L.Z., and Q.T.; visualization, X.L., L.Z., and Q.T.; supervision, L.Z., Q.T.; project administration, X.L. and Q.T.; funding acquisition, X.L. and Q.T. All authors have read and agreed to the published version of the manuscript.

Funding: This research was supported by Scientific and Technologial Innovation Programs of Higher Education Institutions in Shanxi, grant number 2024L214, Fundamental Research Program of Shanxi Province, grant number 202403021222201 and National Natural Science Foundation of China, grant number U24A20136.

Data Availability Statement: The data that support the findings of this study are available from the corresponding author upon reasonable request.

Conflicts of Interest: The authors declare that they have no known competing financial interests or personal relationships that could have influenced the work reported in this paper.

References

1. Wu Dafang, Wang Yuewu, Shang Lan, Pu Ying, Gao Zhengtong. Thermo-mechanical properties of C/SiC composite structure under extremely high temperature environment up to 1500°C[J]. Composites Part B: Engineering, 2016, 90:424-431.
2. Fonseca, Michael, A., English, Jennifer, M., von, Arx, Martin, Allen. Wireless Micromachined Ceramic Pressure Sensor for High-Temperature Applications[J]. Journal of Microelectromechanical Systems, 2002.
3. Tan Qiulin, Lu Fei, Ji Yaohui, Wang Haixing, Zhang Wendong, Xiong Jijun. LC temperature-pressure sensor based on HTCC with temperature compensation algorithm for extreme 1100°C applications[J]. Sensors & Actuators A Physical, 2018: S0924424718308379-.

 doi:10.20944/preprints202505.0882.v1

4. Gregory OJ, Conkle JR, Birnbaum T J. Wireless temperature measurement system and method of using same:, EP2569609 A2[P]. 2013.
5. Tahan M, Tsoutsanis E, Muhammad M, ZAA Karim. Performance-based health monitoring, diagnostics and prognostics for condition-based maintenance of gas turbines: A review[J]. Applied Energy, 2017, 198:122-144.
6. Almasi, Amin. Gas Turbine Engineering Handbook[J]. Chemical Engineering, 2012.
7. Sousa J, Paniagua G, Morata EC. Thermodynamic analysis of a gas turbine engine with a rotating detonation combustor[J]. Applied Energy, 2017, 195(JUN.1):247-256.
8. Wu Dong, Wang Xin, Dong Wenchao, Lu Shanping. Effects of welding thermal cycle and aging treatment on the microstructure and mechanical property of a ni-fe base superalloy[J]. Acta Metallurgica Sinica, 2014, 50(3):313-322.
9. Song Xinyu, Jin Hao, Dong Shurong, Zhang Miling, Zhang jikai, Xu Hongsheng, Chen Jinkai, Xuan Weipeng, Luo Jikui. New composite electrode for high temperature surface acoustic wave device - ScienceDirect[J]. Materials Letters, 2021, 294.
10. Ayes A, Maskay A, Pereira D. Predicted and measured temperature compensated surface acoustic wave devices for high-temperature applications[J]. Electronics Letters, 2017, 53(11):699-700.
11. Fachberger R, Bruckner G, Hauser R, et al. Wireless SAW based high-temperature measurement systems[C]// 2006 IEEE International Frequency Control Symposium and Exposition. IEEE, 2006.
12. Champbell CK. Surface Acoustic Wave Devices for Mobile and Wireless Communications, 1998:631.
13. Wei L, Guo Y, Tang Y, et al. Room-Temperature Ammonia Sensor Based on ZnO Nanorods Deposited on ST-Cut Quartz Surface Acoustic Wave Devices[J]. Sensors, 2017, 17(5):1142.
14. Kadota M , Ishii Y , Tanaka S . Surface Acoustic Wave Resonators With Hetero Acoustic Layer (HAL) Structure Using Lithium Tantalate and Quartz[J]. IEEE Transactions on Ultrasonics Ferroelectrics and Frequency Control, 2020, PP(99):1-1.
15. Zhang Yongwei, Tan Qiulin, Zhang Lei, Zhang Wendong and Xiong Jijun. A novel SAW temperature-humidity-pressure (THP) sensor based on LiNbO3 for environment monitoring[J]. Journal of Physics D: Applied Physics, 2020, 53(37).
16. Shen J, Fu S, Su R, et al. High-Performance Surface Acoustic Wave Devices Using LiNbO3/SiO2/SiC Multilayered Substrates[J]. IEEE Transactions on Microwave Theory and Techniques, 2021, PP (99):1-1.
17. Brugger M S, Schnitzler L G, Nieberle T, et al. Shear-horizontal surface acoustic wave sensor for non-invasive monitoring of dynamic cell spreading and attachment in wound healing assays[J]. Biosensors & Bioelectronics, 2021, 173:112807.
18. M. Kü, Heigl M, Flacke L, et al. Symmetry of the Magnetoelastic Interaction of Rayleigh and Shear Horizontal Magneto Acoustic Waves in Nickel Thin Films on LiTaO3[J]. Physical Review Applied, 2021, 15(3).
19. Aubert T, Kokanyan N, Elmazria O. Langasite as Piezoelectric Substrate for Sensors in Harsh Environments: Investigation of Surface Degradation under High-Temperature Air Atmosphere[J]. Sensors, 2021, 21(17):5978.
20. Aubert T, Elmazria O. Stability of langasite regarding SAW applications above 800°C in air atmosphere[C]// 2012 IEEE International Ultrasonics Symposium. IEEE, 2013.
21. Aubert T, Bardong J, Elmazria O, et al. Iridium interdigital transducers for high-temperature surface acoustic wave applications[J]. Ultrasonics Ferroelectrics & Frequency Control IEEE Transactions on, 2013, 59(2):194-197.
22. Bardong J, Bruckner G , Kraft M, et al. Influence of packaging atmospheres on the durability of high-temperature SAW sensors[C]// Ultrasonics Symposium (IUS), 2009 IEEE International. IEEE, 2009.
23. Xu Fangmeng, Xue Tao, Liang Xiaorui, Tan Qiulin. High-temperature direct bonding of langasite using oxygen plasma activation[J]. Scripta Materialia, 2021, 194(4):113681.
24. Ghosh A, Zhang C, Shi S, et al. High temperature CO2 sensing and its cross-sensitivity towards H2 and CO gas using calcium doped ZnO thin film coated langasite SAW sensor[J]. Sensors and Actuators B: Chemical, 301.

 doi:10.20944/preprints202505.0882.v1

25. Li X , Wang W , Fan S , et al. Optimisation of SAW Devices with LGS/Pt Structure for Sensing Temperature[J]. Sensors, 2020, 20(9):2441.
26. Peng Z, Chin T L, Greve D W, et al. Pulse-mode temperature sensing with langasite SAW devices[C]// IEEE International Frequency Control Symposium. IEEE, 2010.
27. Tiggelaar R M, Sanders R, Groenland A W, et al. Stability of thin Pt films implemented in high-temperature microdevices[J]. Sensors & Actuators A Physical, 2009, 152(1):39-47.
28. Aubert T, Bardong J, Elmazria O, et al. Iridium interdigital transducers for high-temperature surface acoustic wave applications[J]. Ultrasonics, Ferroelectrics and Frequency Control, IEEE Transactions on, 2012, 59(2): p.194-197.
29. Lisker M, T Hur'Yeva, Ritterhaus Y, et al. Effect of annealing in oxygen atmosphere on morphological and electrical properties of iridium and ruthenium thin films prepared by liquid delivery MOCVD[J]. Surface & Coatings Technology, 2007, 201(22-23):9294-9298.
30. K, J, Duxstad, et al. High temperature behavior of Pt and Pd on GaN[J]. Journal of Applied Physics, 1997, 81(7):3134-3134.
31. Behanan R , Moulzolf S C , Call M , et al. Thin films and techniques for SAW sensor operation above 1000°C[C]// IEEE International Ultrasonics Symposium. IEEE, 2014.
32. Liu Xingpeng. The Fabrication and Investigation of Electrodes for SAW Devices Working at High Temperature[D]. University of Electronic Science and Technology of China,2018.
33. Zhou Xuhang, Tan Qiulin, Liang Xiaorui, et al. Novel Multilayer SAW Temperature Sensor for Ultra-High Temperature Environments[J]. Micromachines, 2021,12(6):643.
34. Tapan Pattnayak, Guhapriyan Thanikachalam. Antenna Design and RF Layout Guidelinesp[M].2018.
35. Zerui Sun,Changgen Shi, Li Gao, Sunlang Lin and Wenxuan Li. Thermal physical properties of high entropy alloy Al0.3CoCrFeNi at elevated temperatures[J]. Journal of Alloys and Compounds,2022,901.
36. Jianlei Liu, Qiong Zou, Zhou Zhang, Qiang Zeng, Huanan Peng, Qikun Wang, Qibing Chang. Research on mixed alkaline-earth effect in non-alkali glass substrates for TFT-LCDs[M]. Journal of Non-Crystalline Solids,2022,579.